Geomorphology 217 (2014) 140–151

Contents lists available at ScienceDirect

Geomorphology

journal homepage: www.elsevier.com/locate/geomorph

Airborne and ground-based data sources for characterizing the morpho-structure of a coastal landslide

Candide Lissak [a,*], Olivier Maquaire [a], Jean-Philippe Malet [b], Adnand Bitri [c], Kevin Samyn [c], Gilles Grandjean [c], Céline Bourdeau [d], Philippe Reiffsteck [d], Robert Davidson [a]

[a] Laboratoire LETG-CAEN GEOPHEN, Géographie Physique et Environnement, CNRS UM5 6554, Université de Caen-Basse-Normandie, Esplanade de la Paix, F-14032 Caen Cedex, France
[b] Institut de Physique du Globe de Strasbourg, CNRS UMR 7516, École et Observatoire des Sciences de la Terre, EOST/Université de Strasbourg, 5 rue Descartes, F-67084 Strasbourg, France
[c] Bureau de Recherches Géologiques et Minières, 3 Avenue C. Guillemin, F-45000 Orléans, France
[d] Institut Français des Sciences et Technologies des Transports, de l'Aménagement et des Réseaux, Département GERS — Géotechnique, Environnement, Risques naturels et Sciences de la terre, 14-20 Boulevard Newton, F-77447 Marne la Vallée Cedex 2, France

ARTICLE INFO

Article history:
Received 31 May 2013
Received in revised form 3 April 2014
Accepted 12 April 2014
Available online 21 April 2014

Keywords:
Landslide morphology
Internal structure
Geotechnics
Geophysics
LiDAR
Multi-source data

ABSTRACT

Landslide analysis is increasingly based on the combination of multiple information sources at different spatial and temporal resolutions, spatial coverage, accuracy and acquired using various airborne and terrestrial platforms and geomorphological, geophysical, and geotechnical methods. Morphological mapping and morpho-structure characterization are preliminary steps to analyze the observed and future landslide distributions. The objective of this work is to propose a morpho-structural model of an active landslide complex on the Normandy coast (north-west France) by combining different data sources. The methodology associates field investigation with interpretation of high-resolution topographic and geophysical images. The proposed morpho-structural model highlights the division of the landslide into several morphological features. This division may explain the spatial variability and temporal variability of the slope dynamics.

1. Introduction

Assessment of landslide morpho-structures requires information on the morphology, geometry and internal structure of the stable and unstable slopes (Malet et al., 2002; Quantin et al., 2004; van Westen, 2004; Bonnard, 2006; Travelletti et al., 2009, 2013; Crozier, 2010; Travelletti and Malet, 2012). A morpho-structural model allows delineation of the spatial extent of a landslide and is key information used by local risk managers in France to prepare hazard maps (MATE/METL, 1999). Field surveys and analyses of very-high resolution digital elevation models (VHR DEMs; Jaboyedoff et al., 2010; Razak et al., 2011) can be combined with historical information on landslide displacement (e.g. results of benchmark surveys and aerial photographs interpretation; McKean and Roering, 2004; Glenn et al., 2006; van den Eeckhaut et al., 2007) and information on slope geometry and structure from geotechnical and geophysical investigations (Grandjean et al., 2006; Jongmans and Garambois, 2007). For landslides developed in soft clayish sediments, seismic and geoelectrical surveys have been widely used to image material layering and detect shear surfaces and structural heterogeneities (Bichler et al., 2004; Grandjean and Sage, 2004; Grandjean et al., 2006; Naudet et al., 2008; Travelletti and Malet, 2012), although it remains difficult to investigate a very large landslide (Chambers et al., 2011). Therefore, combining different data sources is useful for characterizing a large landslide complex (Travelletti and Malet, 2012).

The southern coast of England and the northern coast of France along the English Channel (North Sea) are prone to landslides with soft sedimentary rocks (Jurassic marls to Cretaceous chalks) and marine erosion at the foot of coastal cliffs (Hutchinson, 1991; Bromhead and Ibsen, 2004; Jenkins et al., 2011). In Normandy, along the Pays-d'Auge coast, the Cirque des Graves landslide has been reactivated in 1982. Previous studies have demonstrated the complex dynamics of this landslide, related to highly variable slope conditions and the presence of several chalk blocks and low resistance layers (Flageollet and Helluin, 1987; Maquaire, 1990). The landslide also presents a complex hummocky surface morphology with scarps and horst–graben structures.

The objective of this work is to integrate multi-source data to formulate a morpho-structural model of the Cirque des Graves

* Corresponding author. Tel.: +33 2 31 56 61 46.
E-mail address: candide.lissak@univ-paris-diderot.fr (C. Lissak).

http://dx.doi.org/10.1016/j.geomorph.2014.04.019
0169-555X/

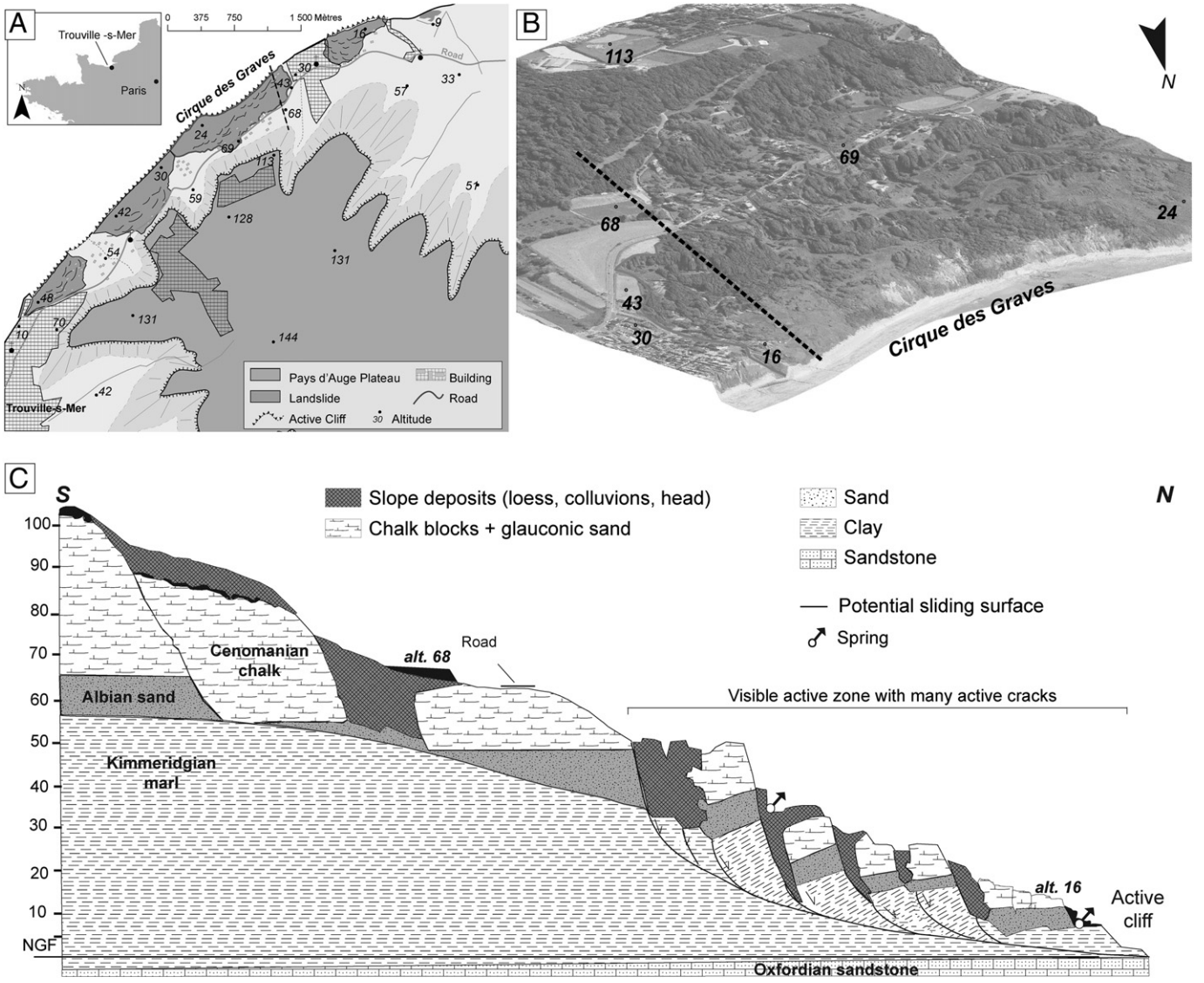

Fig. 1. Geomorphological setting of the Cirque des Graves landslide. (A) Topographic context with location of active landslides along the coast. (B) 3D view of the Cirque des Graves landslide in 2006. (C) Geological cross-section after Flageollet (1989).

landslide. The methodology, combining near-surface geophysical methods, geotechnical drilling and morphologic observations, provides information on: (1) the present state of activity; (2) the main petro-physical and geotechnical characteristics of the landslide material; (3) the volume and geometry of each compartment of the landslide.

2. Study area

Along the edge of the Pays d'Auge coast (north west of France; Fig. 1), several landslides occur below 140 m a.s.l. (Lissak et al., 2013a). These landslides are located on convex–concave slopes in highly-urbanized areas. This work focuses on the Cirque des Graves landslide (municipality of Villerville) which is the most active and largest landslide in this region (47 ha in 2012) and is characterized by the presence of composite rotational slides of >20 m thick (Maquaire, 1990). Four main failure events (Lissak et al., 2014) observed since 1982 have induced damages to buildings and traffic infrastructures (Fig. 2) and have affected the local economy (Lissak et al., 2013a).

The landslide occurs in Jurassic sedimentary rocks with a stratigraphic sequence, from the bottom to the top of: 10 m thick Oxfordian sandstone plunging gently to the south-east (10–20%); 25 m thick Kimmeridgian marl; 3 m thick Albian sand; and 50 m thick (at least) Cenomanian chalk (Maquaire, 1990). The slope surface is partly covered by weathered flint clay and periglacial slope deposits.

The slope was already unstable before the first recent major failure of January 1982 (Flageollet and Helluin, 1987; Lissak et al., 2013b) as indicated by the presence of high scarps (10–15 m high) (Fig. 2A). Three other significant failure events occurred in February 1988, March 1995 and March 2001 (Fig. 2B). In addition to these major failures, average surface displacement rates of 5–10 cm year^{-1} are observed in the landslide accumulation zone (Lissak et al., 2013b, 2014). As a consequence, the resulting topography consists of multiple rotational slides with typical features such as open cracks, fresh scarps, small depressions, counter-slopes and lobes at the toe.

The landslide is monitored since 1985 (Lissak et al., 2010). Prior to this, field investigations focusing on the eastern part of the landslide (Flageollet and Helluin, 1987; Maquaire, 1990) highlighted the role of the displaced chalk blocks on landslide dynamics, and Maquaire

Fig. 2. Example of large scarps created by the 1982 and the 2001 failure events. (A) Example of a destroyed building in 1982. (B) Example of damages to the main road in 2001. (C) New scarp created downhill of a building in 2001.

(1990) proposed a geometrical model of the landslide along a cross-section (Fig. 1C).

3. Methods and data sources

3.1. Methods

The methodology used to define the morpho-structure consists of three steps (Fig. 3). First, we investigated the morphology of the slope surface through aerial orthophotographs and airborne laser data (Haneberg et al., 2009). Then we performed geotechnical drillings and geophysical investigations (seismic and geoelectric acquisitions) along selected cross-sections to characterize the landslide material layering and identify discontinuities (Lissak, 2012). Finally, a morpho-structural model of the slope is proposed by combining the geomorphological, geotechnical, and geophysical models.

3.2. Data

3.2.1. Surface data from airborne and field surveys

To define and characterize the main morphological features (e.g. major, secondary, minor scarps, active cracks, and counter-slopes), we conducted 1) series of field surveys; 2) interpretation of aerial orthophotographs (spatial resolution of 0.30 m) acquired in 2000, 2006, and 2009; and 3) analysis of an airborne LiDAR-derived digital elevation model (DEM) acquired in April 2010. The root mean square error (*RMSE*) was calculated for all geospatial data using 22 control points measured by differential GNSS with a horizontal accuracy of 0.05 m (Kasser and Egels, 2001; Casson, 2002). The control points are easily identified on various geospatial data (Hughes et al., 2005) and located on stable sectors of the slope such as building and street corners, and intersections of roads and pathways. The accuracy of the geometrical correction of the geospatial data in terms of *RMSE* varies between 0.40 m (aerial orthophotograph from 2006) and 0.98 m (aerial orthophotograph from 2000). In the field, morphological features were precisely located by differential GNSS with an accuracy of 0.05 m. Many areas of the landslide, however, could not be directly mapped because of a dense vegetation cover.

An airborne LiDAR point cloud was acquired by the Helimap© company in April 2010 when vegetation coverage was relatively low, using a helicopter flying around 300 m above the ground. To obtain a dense point cloud, seven flight lines approximately parallel to the shore direction were acquired. The average density of the point cloud is 40 ± 15 pts m^{-2} before filtering vegetation, and 4 ± 2 pts m^{-2} after

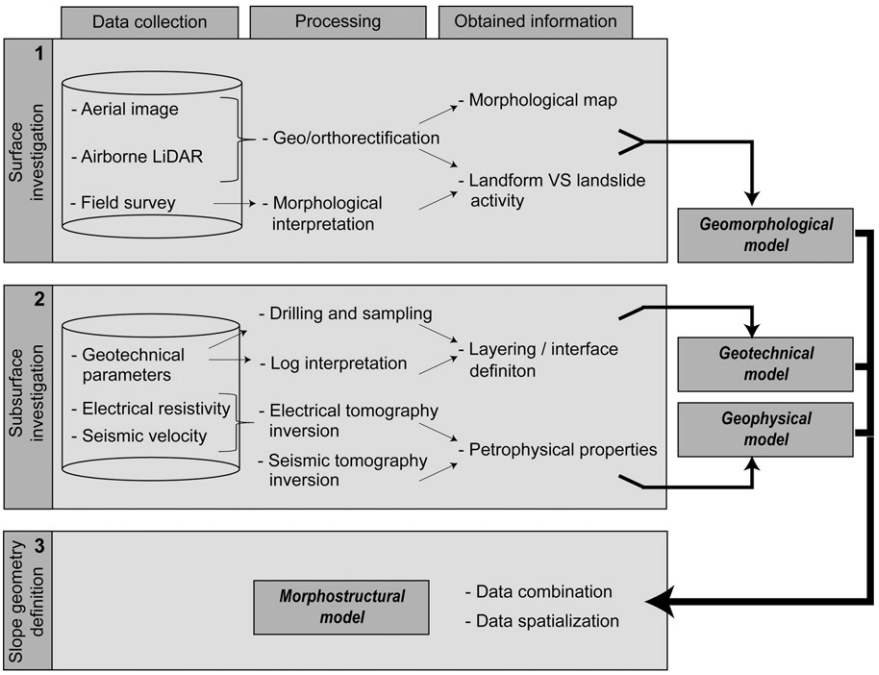

Fig. 3. Methodology used for combining different sources of information and geomorphological, geotechnical and geophysical models to propose a morpho-structural slope model.

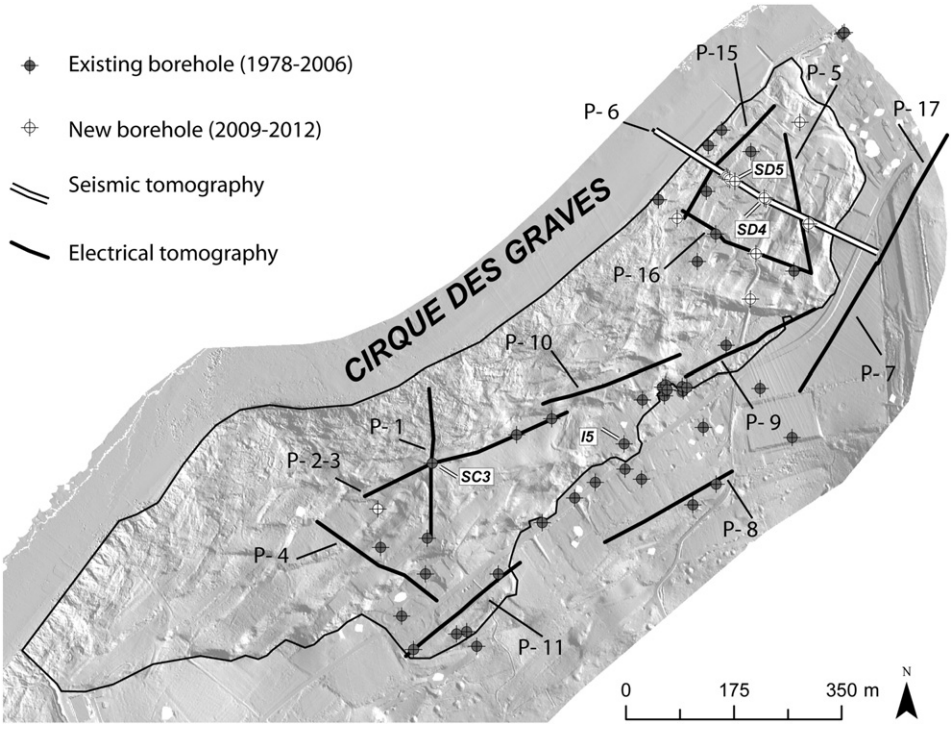

Fig. 4. Hillshade of the slope morphology from a 0.5 m DEM from 2010 airborne LiDAR survey interpolation with locations of the studied cross-sections and boreholes.

filtering. The filtered point cloud was interpolated at a spatial resolution of 0.5 m using the inverse distance weighted (IDW) method. The vertical accuracy of the DEM was determined as *RMSE* of elevation (Z) compared with that measured by differential GNSS. In terrains without forest, the average difference in Z is 0.04 m with an *RMSE* value of 0.01 m, according to the measurements at three ground control points. In forested terrains, the comparison was carried out using a series of ten ground controls points; the average difference in Z was 0.40 with an *RMSE* value of 0.12 m after data filtering. Fig. 4 presents a hillshade view of the airborne LiDAR DEM with the location of the investigated cross-sections and boreholes.

3.2.2. Subsurface data from boreholes

Since 1978, 56 drillings (depths between 2 and 57 m) were carried out. Their locations are presented in Fig. 4. Between 1978 and 2006, 36 drillings were performed and 11 were sampled. Between 2009 and 2011, 20 rotation and percussion drillings were performed and 11 were sampled. For all these new drillings, standard penetration tests have been realized and for five drillings, drilling parameters were recorded such as the downthrust pressure (P_o), the vertical progress rate (V_a), the rotation rate (V_r), and the retaining pressure (P_v). These parameters are used to calculate the Somerton index (Somerton, 1959) to identify the nature and layering of the rock (da Fonseca and Coelho, 2007) and to indirectly infer some mechanical properties (Laudanski et al., 2012). An example of drilling records is shown in Fig. 5.

3.2.3. Subsurface data from electrical resistivity and seismic tomographies

Cross-section P-6 (see Fig. 4 for the location) was investigated using both electrical resistivity tomography (ERT) and seismic refraction tomography, while the other cross-sections were investigated only with ERT. The locations of the slope-parallel and slope-perpendicular cross-sections were selected to interrogate the boundaries of the landslide, to cross several chalk blocks and are close to the wettest surface areas. For ERT, a Wenner–Schlumberger configuration was used to measure

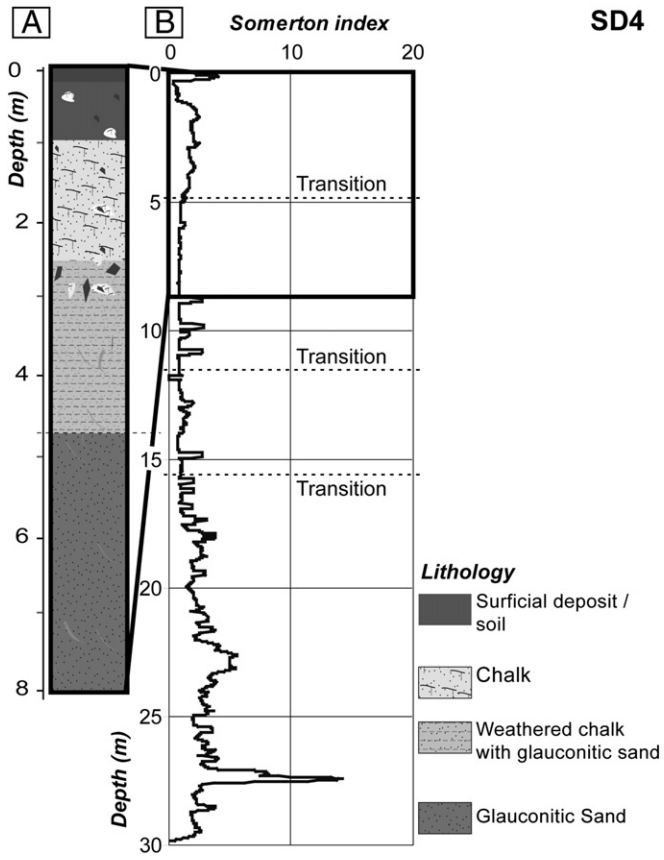

Fig. 5. Examples of core-sampled and individual profile obtained for the SD4 borehole using the Somerton Index. (A) Material layering and structure determined from sampling. (B) Vertical profile of the Somerton index and interpretation of material layering. The location of borehole is shown in Fig. 4.

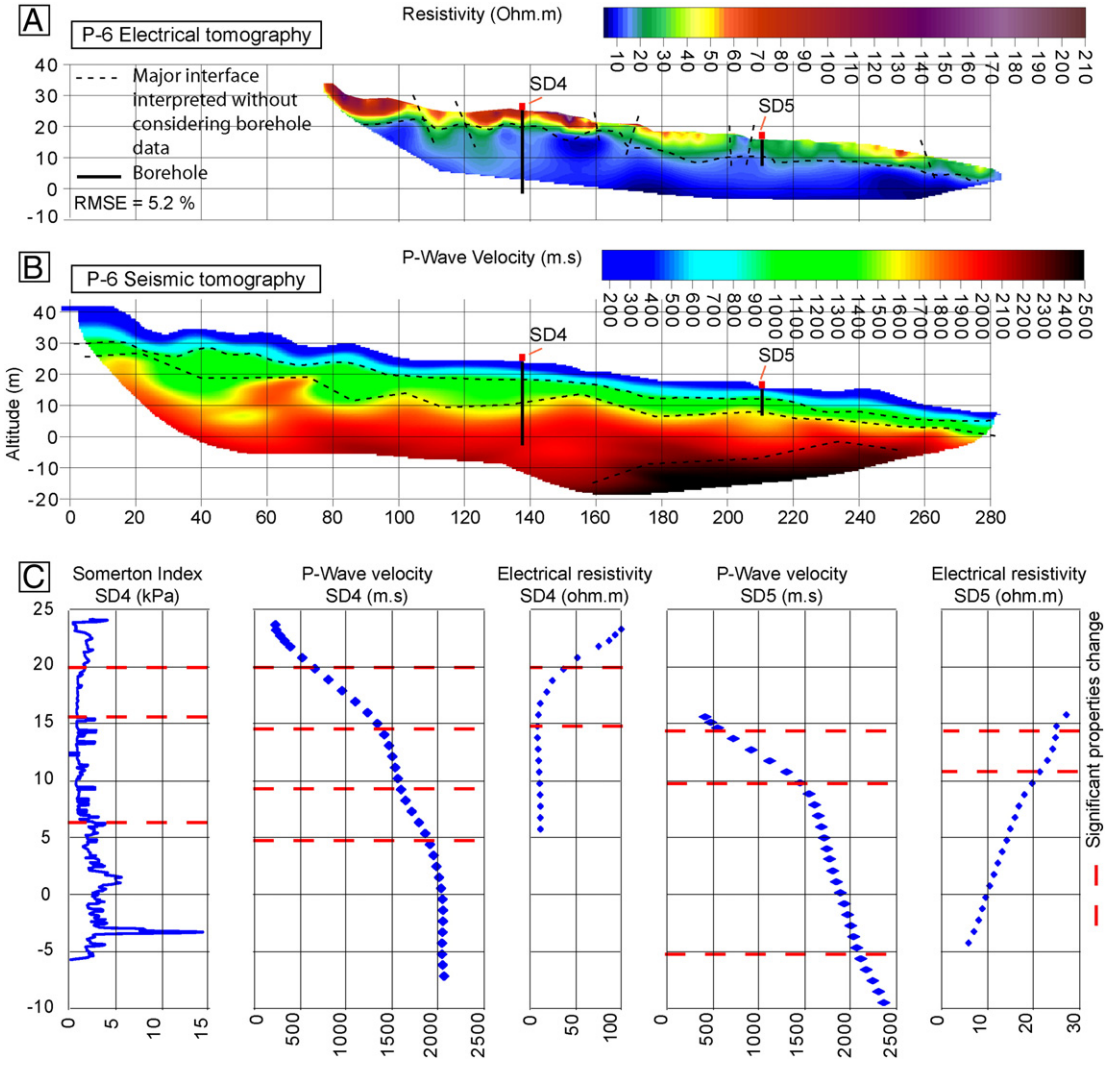

Fig. 6. Slope morphology and geotechnical model along the cross-section P-6 in the eastern part of the Cirque des Graves landslide. (A) Geological cross-section interpreted from the geotechnical drillings and the slope morphology. (B) Electrical resistivity model. (C) Seismic P-wave velocity model.

the apparent resistivity and increase the depth resolution (Schrott and Sass, 2008). The effectiveness of this configuration has already been demonstrated in landslide research especially for highly heterogeneous structures (Naudet et al., 2008; Jongmans et al., 2009). The acquisition profiles have a length of 240 m, and are composed of 48 electrodes each spaced 5 m apart. An IRIS-Syscal Junior resistivimeter (48 channels; accuracy of the electrical current measurement of 0.5%) was used. The 2D sections of apparent resistivity (Fig. 6) were processed using the least mean square method (Loke, 1999) with the RES2DINV software, and *RMSE* values for the inverted resistivity were between 0.6% and 6.7% after three iterations.

The seismic tomography profile was over 280 m long and comprising 134 (10-Hz) geophones at 2 m spacing. Detonating cord (100 g) was used to perform 27 shots, 6 m away from the cross-sections. Seismic tomography allows imaging of 2D structures of P-wave seismic velocity. The quasi-Newton P-wave tomography inversion algorithm developed by Gance et al. (2012) was used to invert the velocity fields. The algorithm is based on the finite frequency assumption for highly heterogeneous media, and considers an objective inversion regularization based on the wave propagation principle. It uses the entire source frequency spectrum to improve the tomography resolution. The Fresnel wave paths calculated for different source frequencies are used to retro-propagate the travel time residuals, assuming that in highly heterogeneous media, the first arrivals are only affected by the velocity anomalies present in the first Fresnel zone.

4. Results and discussion

4.1. Surface investigation: geomorphological model

The slope geometry was defined by combining the geomorphological, geotechnical and geophysical models to characterize the morpho-structural units in terms of presence, size and thickness of chalk blocks.

As shown in Fig. 7, the main morphological features characterizing landslide activity were identified in the field and in the LiDAR DEM. These features were classified into two categories according to the type and depth of the processes. The first category includes features in landslide source areas (types A to F) with major scarps related to major failure events, secondary and minor scarps and also recent fissures linked to seasonal displacements. The second category corresponds to morphological features of the landslide deposition areas (types G and H). These features are related to shallow mudflows at the surface.

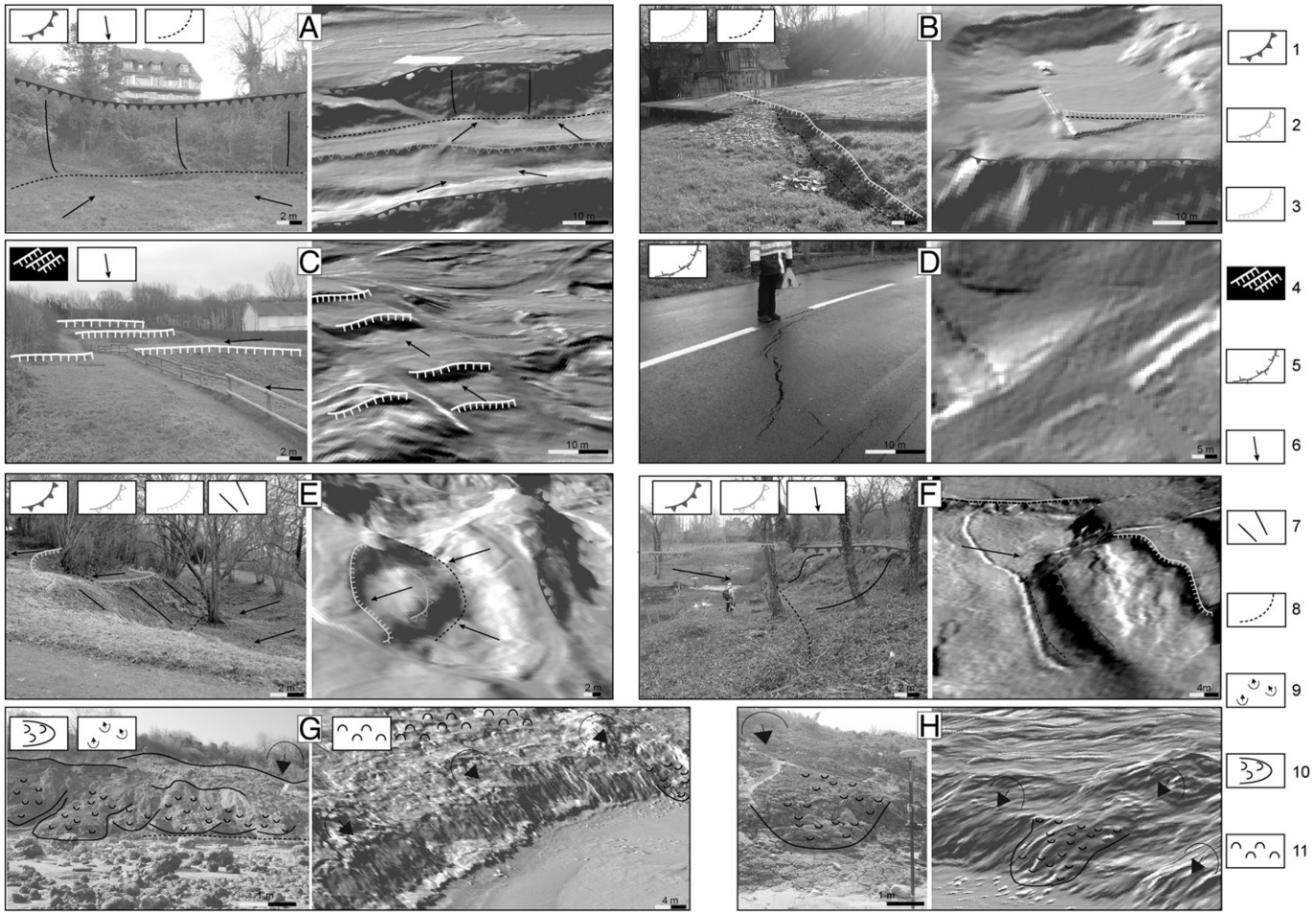

Fig. 7. Morphological features characterizing the landslide activity, and associated field photographs and signatures in the LiDAR DEM. (A) Major scarps >5 m high, related to the intense activity of the landslide. (B) Secondary scarps, 2–5 m high, related to the last 30 year activity. (C) Minor scarps covered by vegetation and related to earlier activity. (D) Fissures which can be easily hidden by the vegetation and slope deposits. (E) Counter-slopes. (F) Small depressions at the base of the major scarps, indicating a rotational component of the displacement. (G) Mudflows deposits. (H) Shallow landslides occurring in the slope deposits at the toe of the landslide. Legend: (1) major scarp more than 5 m high, (2) secondary scarp between 2 and 5 m high, (3) minor scarp between 0.5 and 2 m high, (4) succession of major and moderate scarps, (5) open fracture, (6) counter-slope, (7) steep slope, (8) slope break, (9) shallow slide, (10) mudflow, and (11) hummocky ground.

The landslide geomorphological map is presented in Fig. 8. The spatial distribution of the morphological features suggests that the landslide body can be divided into four distinct units. 1) The uphill and western parts of the landslide are characterized by scarps of several hundred meters in length and 5–10 m high, more or less parallel and perpendicular to the slope direction. Most of these had already been identified in historical documents before the main failure event of 1982 (Lissak et al., 2013b). 2) The eastern part of the landslide is characterized by a very chaotic topography consisting of scarps, more abundant than in the rest of the landslide but smaller in terms of height and length. This part of the landslide was the area most affected by the failure event in January 1982. 3) Another unit on the western side is considered as the less active part of the landslide, and consists of a hummocky terrain with no major scarps. 4) The fourth unit concerns the landslide toe affected by slope dynamics different from those affecting the upper units, with shallow slides and mudflows close to the shoreline.

4.2. Subsurface investigation

4.2.1. Slope geometry and lithofacies

Drilling data from the last 30 years were reinterpreted according to the description of the recent drillings. Five lithofacies were defined based on the analysis of borehole sediments, measurement of the Somerton index, and in-situ pressiometer tests. From the top to the bottom, the lithofacies are:

(1) Superficial deposits composed of a mixture of weathered fragments of the chalk formation. Weathered chalk and clay with flint are present in a silty matrix of head units (sandy with chalk pebbles; Journaux, 1971; Flageollet and Helluin, 1984, 1987). The thickness of these deposits varies from a few decimeters to several tens of meters.
(2) The Cenomanian chalk, widely weathered and fractured into different blocks of varying sizes. These elements, whose thickness varies between 2.5 and 18.0 m, constitute the principal aquifer with the underlying sandy formations. Small chalk blocks are incorporated into a head formation, and the largest blocks are covered by head and loess.
(3) The glauconitic sands at the base of the chalk, characterized by high porosity and low cohesion. The thickness of the sands varies on each side of the slope, between 1.0 and 20.0 m.
(4) The Kimmeridgian marls, outcropping at the toe, and affected by shallow mudflows. The marls are characterized by the presence of thin clay layers (Hutchinson and Bromhead, 2002; McInnes, 2005).

The forth unit is underlain by Oxfordian sandy limestone and sandstone that constitute the flat rocky reef.

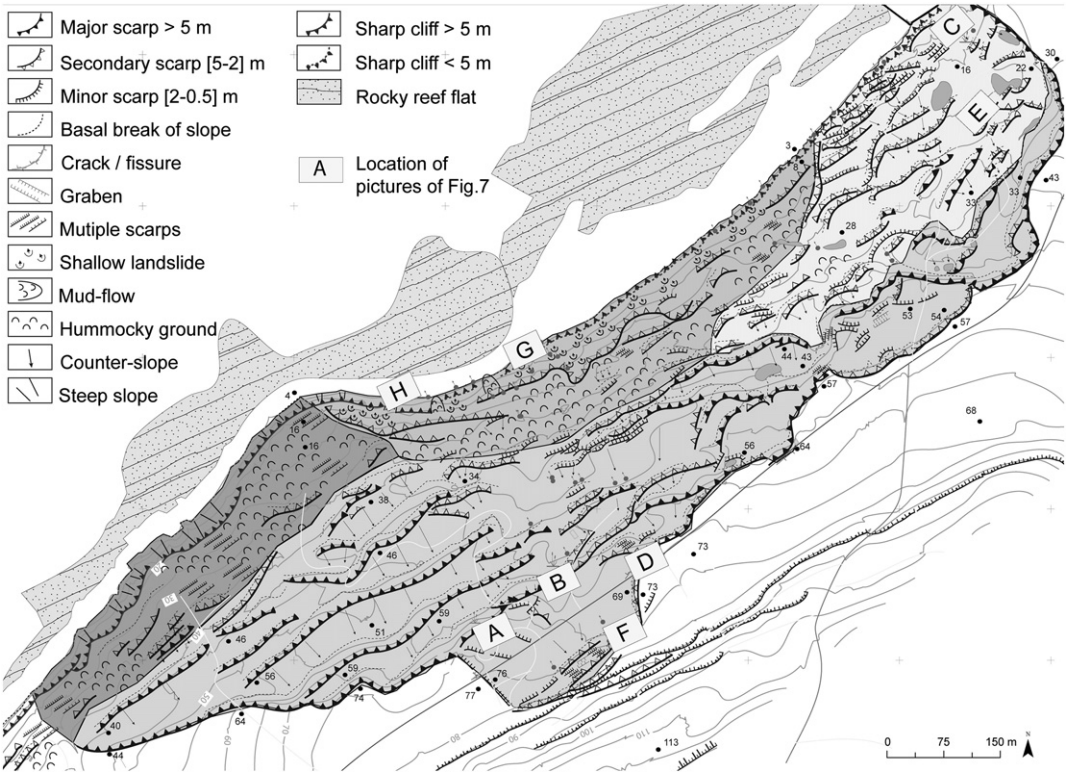

Fig. 8. Geomorphological map of the landslide representing the slope features observed in 2010.

The shear surfaces are identified in most of the boreholes, and are located in the Kimmeridgian marls at depths of ca. 5 m at the downhill sectors and 18 to 23 m at the uphill sectors. The area is also affected by superficial deformation as indicated by additional shear surfaces in some boreholes such as in I5 (Fig. 4) where two shear surfaces have been detected at 7 and 12 m depths in the silty–clay material.

4.2.2. Geophysical structure

Interpretation of the electrical and seismic tomography is based on: (1) abrupt vertical and horizontal changes of apparent resistivity and P-wave velocity; (2) identification of discontinuities in the borehole logs; and (3) record of drilling parameters. Within the landslide, the apparent resistivity values are between 10 and 500 Ωm. In a vertical plane, significant changes can be observed in relation to the petrophysical properties categorized using the Somerton index (Fig. 6). Fig. 9 illustrates the spatial distribution of the resistivity, with significant contrast between the eastern and western sectors. The eastern sector, especially its uphill part, is characterized by low resistivity values, while the western part is characterized by higher resistivity values associated with the presence of chalk blocks.

A resistivity model in three units is proposed (Table 1). The first unit (C) corresponds to the highest resistivity values between 100 and 500 Ωm. These values are associated with the chalk formation which has different degrees of porosity and water content. This unit consists

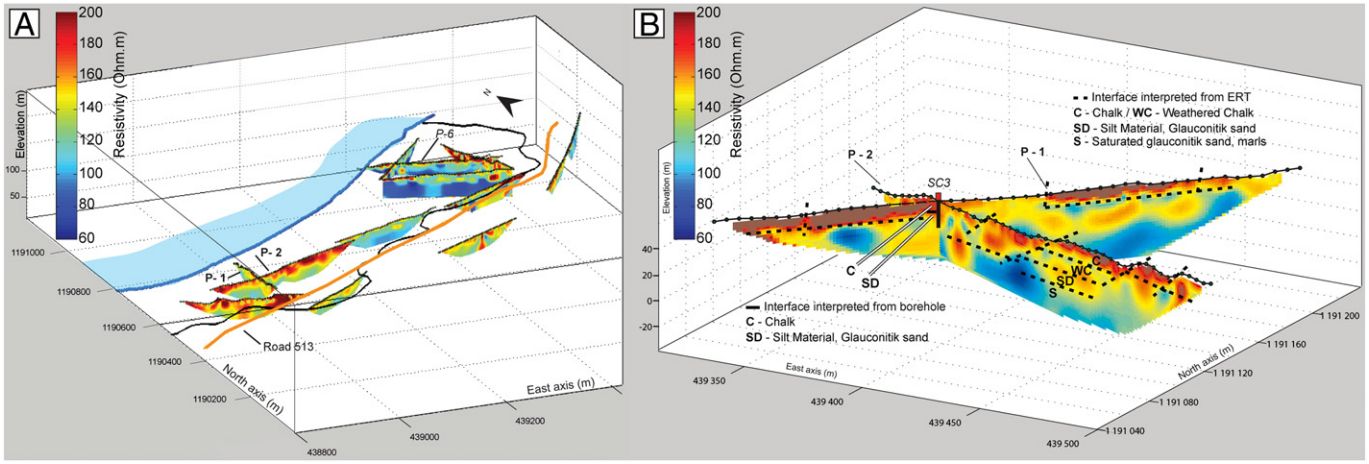

Fig. 9. Proposed resistivity model of the Cirque des Graves landslide (A), and focus on profiles P-1 and P-2 (B).

Table 1
Interpretation of apparent resistivity and seismic P-wave velocity at the location of the SD4 borehole.

Depth (m)	Resistivity (Ωm)	Lithofacies
0–5	100–500	Weathered chalk/surficial formation/ unsaturated material
	60–100	Silty material surrounding the chalk blocks
5–10	<60	Saturated material, sand
Depth (m)	**P-wave velocity (ms)**	**Lithofacies**
0–5	200–600	Weathered chalk/surficial formation/ unsaturated material
5–10	600–1200	Saturated material, sand
10–20	1200–1800	Saturated clay material,
>20	1800–2000	Marl
	>2000	Sandstone

of a combination of competent chalk or weathered chalk (WC). As can be observed on Profile P-6 (Fig. 6), the main chalk blocks are easily differentiated from the surrounding materials. Fig. 9B highlights the boundaries between the chalk blocks surrounding high conductivity materials and/or saturated layers. The second unit (SD), with resistivity values between 60 and 100 Ωm, corresponds to the silty material surrounding the chalk blocks, and consists of a combination of weathered chalk and the glauconitic sands. The third unit (S), with resistivity values less than 60 Ωm, corresponds to the saturated glauconitic sand and marls.

The seismic tomography highlights a heterogeneous slope structure, characterized by vertical organization of the P-wave velocity, increasing with depth from 150 to 2500 m s^{-1}. Longitudinal organization of the P-wave velocity (Fig. 10) coincides with the series of scarps observed at the slope surface. A seismic model in four units is proposed, and can be associated with the lithofacies (Fig. 10). The first unit, with P-wave velocity values between 200 and 400 m s^{-1}, corresponds to surficial deposits a few meters thick. The second unit, with P-wave velocity values between 600 and 1600 m s^{-1}, gradually increasing with depth, corresponds to the chalk block and to the glauconitic sands. The third unit, with P-wave velocity values between 1600 and 2200 m s^{-1}, corresponds to the marls. The fourth unit, with P-wave velocity greater than 2200 m s^{-1}, corresponds to the sandstone bedrock. The observed values of P-wave velocity are similar to those identified in the literature for similar landslide materials (Mauritsch et al., 2000; Glade et al., 2005; Grandjean et al., 2006).

4.3. Morpho-structural model of the slope geometry

The integration of all available information allows proposing a morpho-structural model of the unstable slope. A morpho-structural map is presented in Fig. 11 and further interpretative cross-sections are detailed in Fig. 12.

The geomorphological map (Fig. 8) allows division of the landslides into 136 morpho-structural units according to morphological and topographical criteria (Fig. 11). The surface limits are defined according to the observed morphological features (Fig. 7). The limits in depth are determined from borehole information, the resistivity model, and inclinometer data. We further consider that the size and distribution of the morpho-structural units along the slope control the observed spatial variability in the surface displacement. A certainty index (varying from 1 to 3) is used to estimate the presence of a chalk block for each morpho-structural unit. The criteria used to define the index are presented in Table 2.

The high (3) and moderate (2) certainty values are attributed to 113 units, while a low (1) certainty value is attributed to 23 units. The size of chalk blocks (e.g. expressed in terms of surface) varies between 100 and 32,000 m^2 with a median of 1496 m^2; the majority of the blocks have sizes less than 3000 m^2.

A spatial pattern of the units can be observed in terms of thickness from east to west and from uphill to downhill (Fig. 11). A decrease in thickness is observed from uphill to downhill because of the progressive fragmentation of the material toward the toe. In the upper region, blocks are more than 10 m thick according to the geotechnical, geophysical, and geomorphological observations along the scarps. Further downhill, the chalk blocks are thinner (<5 m thick). In the western area, large and deep blocks more or less parallel to the coastline are

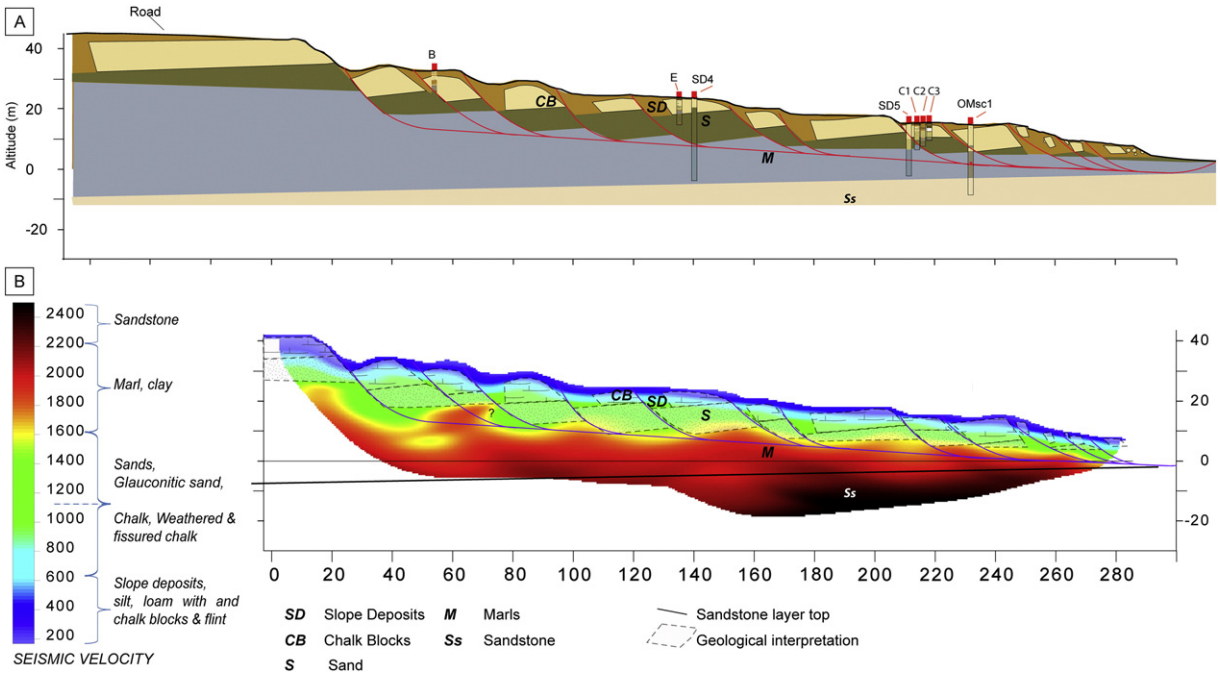

Fig. 10. Proposed seismic P-wave velocity model of the northern part of the Cirque des Graves landslide (cross-section P-6).

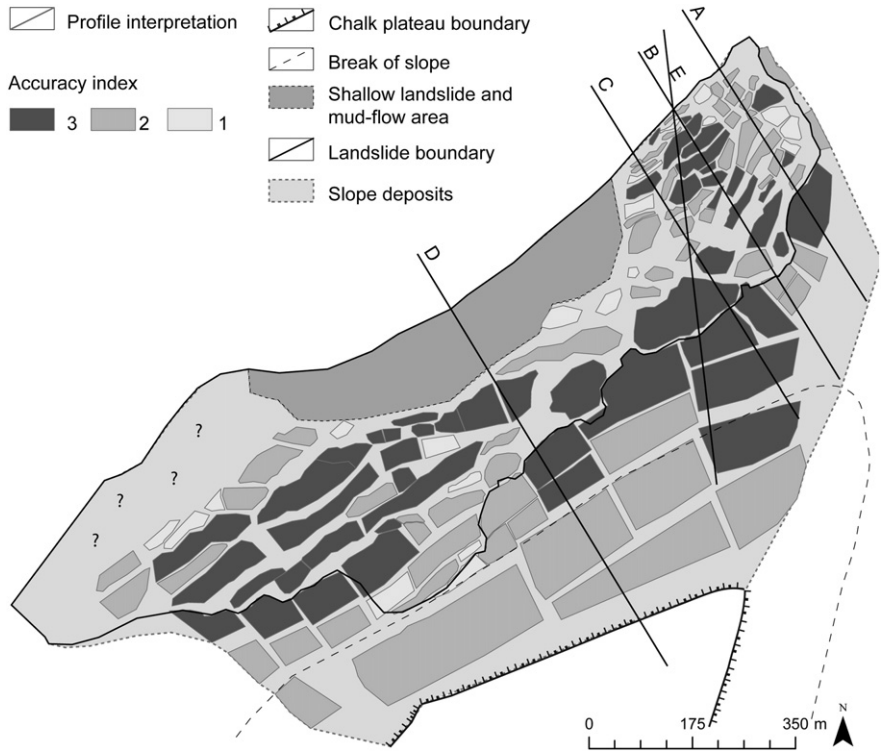

Fig. 11. Morpho-structural model of the Cirques des Graves landslide, and proposed delineation of sub-units corresponding to the chalk blocks.

observed, and underlined by a steep topography with high scarps (5–15 m height) delimiting slightly tilted large components (10,000–23,000 m^2). The most active part in the east is characterized by a chaotic topography with numerous fragmented units (200–5000 m^2) delineated by scarps of moderate heights (3–10 m). The toe of the landslide is a single morpho-structural unit affected by shallow slides and mudflows. In this unit, the slope material consists of small blocks of highly weathered chalk materials embedded in a silty–clay matrix (Fig. 11).

Interpretation of the cross-sections (Fig. 12) clearly demonstrates the complexity of the landslide geometry. The principal shear surface is limited in depth by the sandstone bedrock. Succession of scarps along all the cross-sections suggests the presence of several nested chalk blocks, which are progressively more fragmented downhill (Fig. 12). Most blocks are tilted and overlay the glauconitic sands. From one unit to another, or within a same unit, the sand layer thickness varies between 0 and 10 m.

4.4. Volume estimates for the morpho-structural units

The theoretical maximum volume of each morpho-structural unit is estimated using the sloping local base level (SLBL) method. This method delineates the potential erodible volume by assuming that all undercut slopes are unstable (Jaboyedoff et al., 2004, 2009; Travelletti et al., 2010). The surface above which the slope material can be eroded by landsliding is determined by following a routine using the elevation of several points of a DEM, which are replaced by the mean value of the altitude of its neighbors (Jaboyedoff et al., 2004). In soft-sediment slopes, this baseline, which corresponds to a potential shear surface, can be curved. The baseline surfaces have been calculated along eight cross-sections by defining a number of invariant points at the slope surface (e.g. position of the shoreline at the toe, main scarp uphill) and in depth (e.g. position of the shear surfaces measured in the inclinometers). The results are shown in Fig. 13. The topography observed in 2010 is used as the initial surface geometry, and a new topography is constructed iteratively by removing the consecutive units from the base to the top of the slope for an average of seven distinct units per cross-section; a baseline surface has been calculated for each unit removed. As the landslide is affected by a retrogressive evolution pattern, the successive removal of units allows the estimation of the potential slope profile in the case of failure. To define a curved shear surface in agreement with the inclinometer data (between 5.5 and 22.5 m deep), three or four tests were required for the eight cross-sections according to the interpolation parameters (curvature tolerance and maximum thickness of the slip surface). Along one cross-section, no multiple baselines can be calculated; if seven units are defined, seven baselines are progressively calculated, and each is dependent on the previous baseline. At least 12 baseline surfaces can be calculated for each cross-section. Using this procedure, the total volume of the landslide is estimated to be 3.0×10^7 m^3, while the volume of each unit varies between 4000 and 400,000 m^3 (Fig. 13), with smaller units occurring at the toe and the eastern part of the landslide.

5. Conclusion

The objective of this work was to propose a morpho-structural model and estimate the volume of the Cirque des Graves landslide from the integration of multi-source surface and sub-surface data. The data available for this site are numerous and of variable quality which should be checked before integration into a geometrical model. While preliminary investigations focused only on the eastern part of the landslide, recent investigations allow us to extend the knowledge to the entire slope structure. The integration of seismic and electrical tomography information with geotechnical investigations allows interpolation of a four-layer geological model of the landslide. In addition, by combining surface and sub-surface data, the landslide body can be sub-divided into several units. Each compartment is delineated according to both surface morphological features and geophysical depth information. The presence of chalk blocks is demonstrated, and their properties (size, thickness, and volume) can be associated with different dynamics

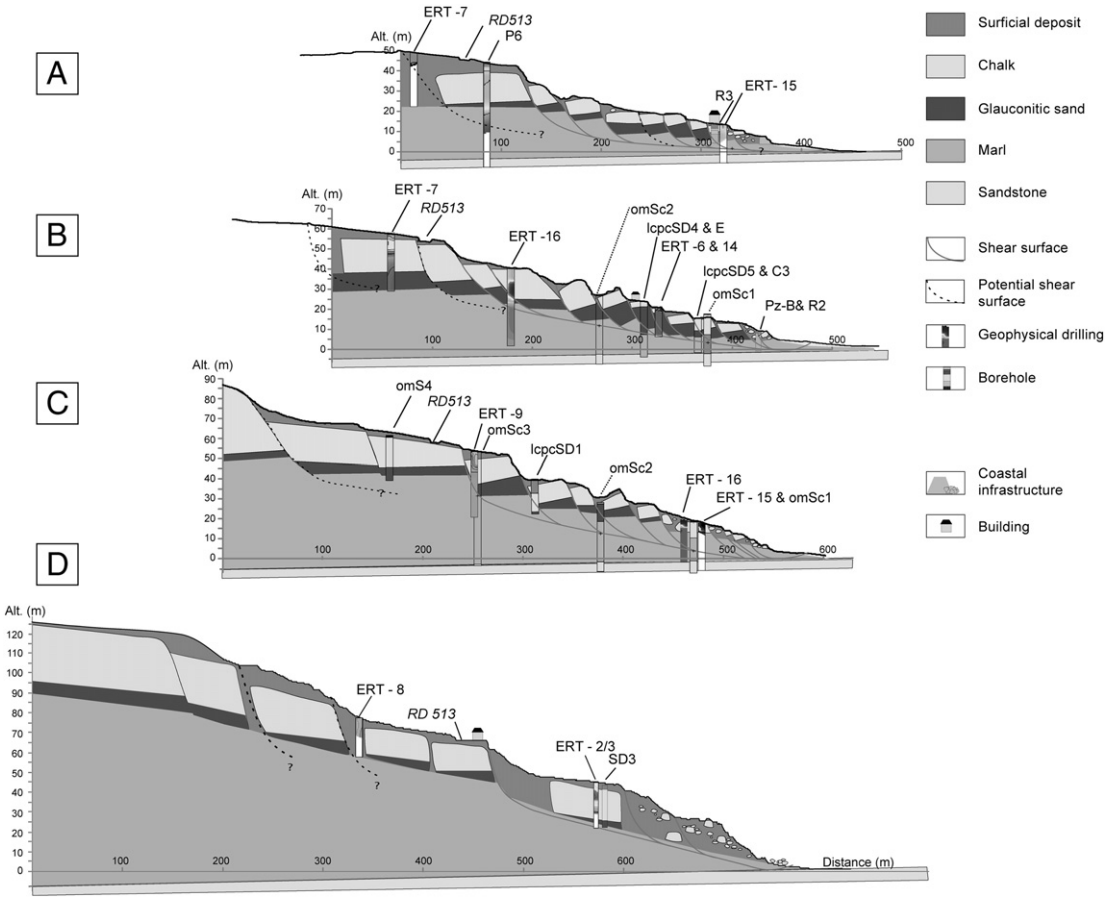

Fig. 12. Cross-sections of the morpho-structural model for the Cirque des Graves landslide (location shown in Fig. 11). (A) Cross-section of the eastern part of the landslide where chalk block thickness decreases because of proximity to the valley. (B and C) Sections though the area most affected during the last 30 years, where chalk blocks have been significantly modified. The smaller width and thickness of the blocks reflect the significant landslide activity in this part. (D) Cross-section of the central part of the landslide, where landslide displacement was relatively small. The morphology of this area is characterized by high and wide scarps with thick and nested chalk blocks. The bottom of the section is affected by mudflows, where small and highly weathered chalk blocks are mixed with silty–clay material.

of the slope and spatio-temporal variability of the displacement rates. A decrease in thickness of the chalk material is observed uphill to downhill to the progressive sliding and fragmentation of the material. While the less active western area is characterized by large, deep, and tilted units, the eastern part is characterized by a chaotic topography with numerous fragmented units. To specify the landslide geometry, the theoretical maximum volume of each morpho-structural unit has been estimated using the SLBL method. The total volume of landslide material is estimated to be 3.0×10^7 m^3. To improve the results of this investigation, 3D geographic data could be implemented to construct an accurate 3D geometrical model, which would complement a geotechnical model to enable analysis of the slope failure initiation and models for post-failure landslide analysis.

Acknowledgments

This research was funded through the RiskNat project 'SISCA: *Système intégré de Surveillance de Crises de glissements de terrain argileux*' (2009–2013) of the *Agence Nationale de la Recherche* (ANR-08-RISK-0009) and the Project CPER GR2TC: *Gestion des Ressources, Risques et Technologie du domaine Côtier*' (2007–2013). The permanent GNSS system and the automated processing of the observations have been setup

Table 2
Certainty index assigned to justify the presence of a chalk block.

Index value	Number of criteria	Criteria
1 — low certainty	<2	Typical slope morphology at the surface (horizontal or slightly back-tilted surface) Observation of chalk in depth in a borehole
2 — moderate certainty	≥2	Typical slope morphology at the surface (horizontal or slightly back-tilted surface) Observation of chalk in depth in a borehole Petro-physical property values representative of chalk
3 — high certainty	>3	Typical slope morphology at the surface (horizontal or slightly back-tilted surface) Observation of chalk at the surface along a scarp Observation of chalk in depth in a borehole Petro-physical property values representative of chalk

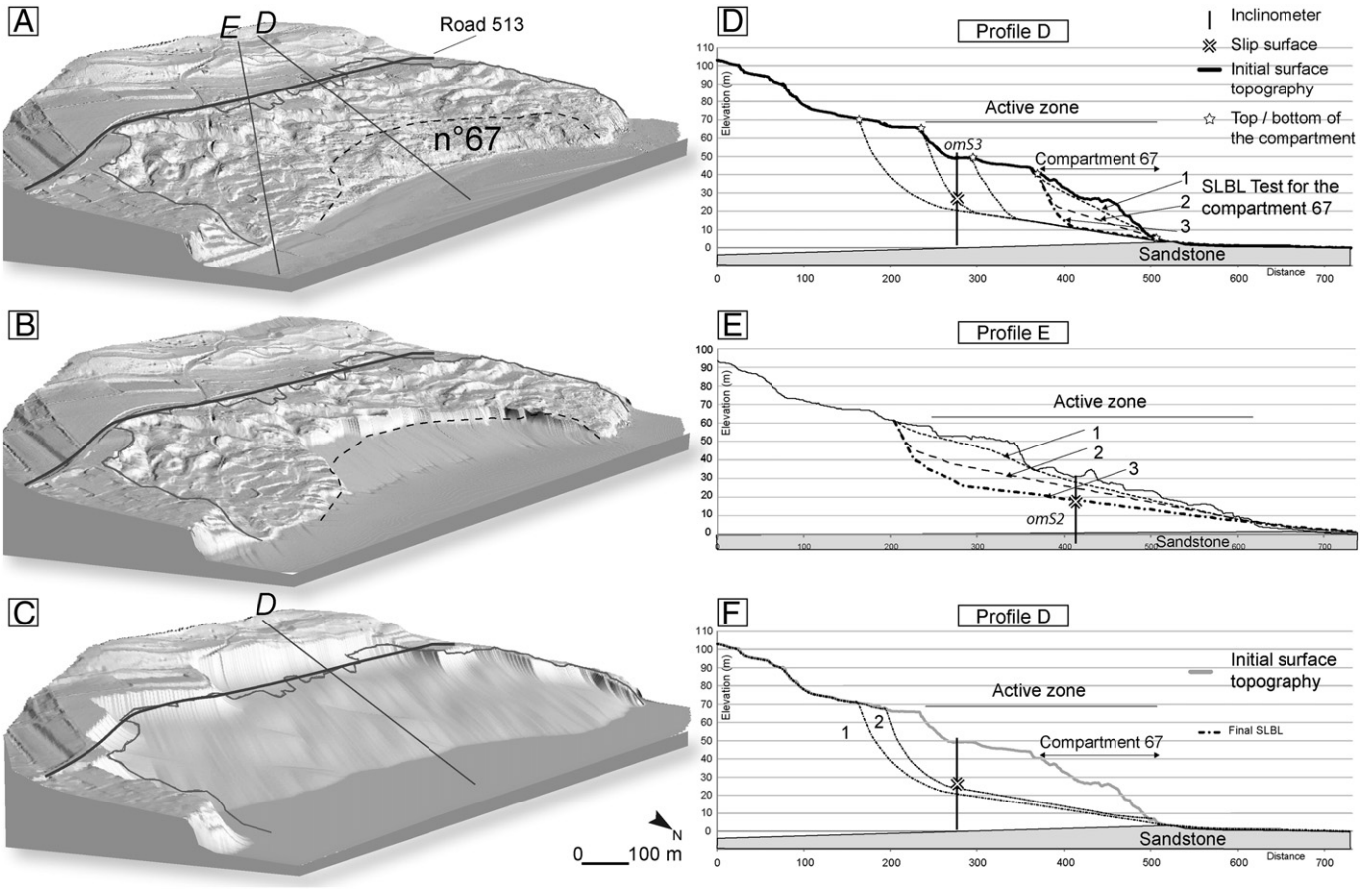

Fig. 13. 2D and 3D representations of potential failure surface depth with the use of the SLBL method. (A) DEM with location of the selected profiles for SLBL calibration and the delineation of one of the compartments (step 0 of the SLBL). (B) DEM with two compartments removed (step 3). (C) DEM with all compartments removed (final step). (D) Profile D with location of multiple baselines calculated using inclinometer data. (E) Profile E with location of multiple baselines calculated using inclinometer data. (F) Profile E with the finale topography. The final topography corresponds to the shear surface that is visible after the removal of all compartments.

by the OMIV-EOST Unit at University of Strasbourg as part of the French Observatory on Landslide. We would also like to thank the LETG-Caen Geophen laboratory team for helping us to install the device.

References

Bichler, A., Bobrowsky, P., Best, M., Douma, M., Hunter, J., Calvert, T., Burns, R., 2004. Three-dimensional mapping of a landslide using a multi-geophysical approach: the Quesnel Forks landslide. Landslides 1, 29–40.

Bonnard, C., 2006. Évaluation et prédiction des mouvements des grands phénomènes d'instabilité de pente. Bulletin für Angewandte Geologie 11 (2), 89–100.

Bromhead, E.N., Ibsen, M.L., 2004. Bedding-controlled coastal landslides in Southeast Britain between Axmouth and the Thames Estuary. Landslides 1, 131–141.

Casson, B., 2002. Apports de l'imagerie optique haute résolution pour l'étude 3D des glissements de terrain. (Ph.D Thesis) University of Lyon p. 1 (281 pp.).

Chambers, J.E., Wilkinson, P.B., Kuras, O., Ford, J.R., Gunn, D.A., Meldrum, P.I., Pennington, C.V.L., Weller, A.L., Hobbs, P.R.N., Ogilvy, R.D., 2011. Three-dimensional geophysical anatomy of an active landslide in Lias Groupmudrocks, Cleveland Basin, UK. Geomorphology 127, 472–484.

Crozier, M.J., 2010. Landslide geomorphology: an argument for recognition, with examples from New Zealand. Geomorphology 120, 3–15.

da Fonseca, A.V., Coelho, S., 2007. Characterization of variable weathered profiles by using DPR. In: Olalla, C., Grossmann, N., Ribeiro de Sousa, L. (Eds.), Proceedings 11th Congress of the International Society for Rock Mechanics. Taylor & Francis, pp. 187–195.

Flageollet, J.C., 1989. Les mouvements de terrain et leur prévention, Masson editions. Collection Géographie, Paris (224 pp.).

Flageollet, J.C., Helluin, E., 1984. Formations quaternaires et zonage des risques de glissements de terrain à Villerville et à Cricquebœuf (Calvados). Colloque «Mouvement de terrain», 22–24 mars 1984. Documents du BRGM, 83, pp. 29–40.

Flageollet, J.C., Helluin, E., 1987. Morphological investigations in the sliding areas along coast of Pays d'Auge, near Villerville, Normandy, France. In: Gardiner, V. (Ed.), International Geomorphology, vol. 1. John Wiley and Sons, Chchester, pp. 447–486.

Gance, J., Grandjean, G., Samyn, K., Malet, J.P., 2012. Quasi-Newton inversion of seismic first arrivals using source finite bandwidth assumption: application to landslides characterization from velocity and attenuation fields. J. Appl. Geophys. 87, 94–106.

Glade, T., Stark, P., Dikau, R., 2005. Determination of potential landslide shear plane using seismic refraction: a case study in Rheinhessen, Germany. Bull. Eng. Geol. Environ. 64, 151–158.

Glenn, N.F., Streutker, D.R., Chadwick, D.J., Thackray, G.D., Dorsch, S.J., 2006. Analysis of LiDAR-derived topographic information for characterizing and differentiating landslide morphology and activity. Geomorphology 73, 134–148.

Grandjean, G., Sage, S., 2004. JaTS: a fully portable seismic tomography software based on Fresnel wavepaths and a probabilistic reconstruction approach. Comput. Geosci. 30, 925–935.

Grandjean, G., Pennetier, C., Bitri, A., Meric, O., Malet, J.P., 2006. Caractérisation de la structure interne et de l'état hydrique de glissements argilo-marneux par tomographie géophysique: l'exemple du glissement-coulée de Super-Sauze, Alpes du Sud, France. C. R. Geosci. 338, 587–595.

Haneberg, W.C., Cole, W.F., Kasali, G., 2009. High-resolution LiDAR-based landslide hazard mapping and modeling, UCSF Parnassus Campus, San Francisco, USA. Bull. Eng. Geol. Environ. 68, 263–376.

Hughes, M.L., McDowell, P.F., Marcus, A.W., 2005. Accuracy assessment of georectified aerial photographs: implications for measuring lateral channel movement in a GIS. Geomorphology 74, 1–16.

Hutchinson, J.N., 1991. Theme lecture. The landslides forming the South Wight Undercliff. In: Chandler, R.J. (Ed.), International Conference on Slope Stability Engineering—Developments and Applications. Thomas Telford, London, pp. 157–168.

Hutchinson, J.N., Bromhead, E.N., 2002. Keynote paper: Isle of Wight. In: McInnes, R.G., Jakeways, J. (Eds.), International Conference on Instability: Planning and Management: Seeking Sustainable Solutions to Ground Movement Problems. Proceedings of the International Conference Organised by the Centre for the Coastal Environment, Isle of Wight Council, and Held in Ventnor. Isle of Wight, UK on 20–23rd May 2002. Thomas Telford, London, pp. 3–70.

Jaboyedoff, M., Baillifard, F., Couture, R., Locat, J., Locat, P., 2004. Toward preliminary hazard assessment using DEM topographic analysis and simple mechanical modeling by means of sloping local base level. Symposium 1. Advances in Geomorphological Mapping. In: Lacerda, W.A., Ehrlich, M., Fontoura, A.B., Sayao, A. (Eds.), Landslide Evaluation and Stabilization, Proceeding 9th International Symposium on Landslides. Bamelka, Rio de Janeiro, pp. 199–205.

Jaboyedoff, M., Couture, R., Locat, P., 2009. Structural analysis of the Turtle Mountain Alberta using DEM: toward a progressive failure by toppling of gently dipping wedges. Geomorphology 103, 5–16.

Jaboyedoff, M., Oppikofer, T., Derron, M.H., Horton, P., Loye, A., Metzger, R., Pedrazzini, A., 2010. Use of LiDAR in landslide investigations: a review. Nat. Hazards 61, 5–28.
Jenkins, G.O., Foster, C., Hopson, M.P., 2011. Geology as a control on landslides on the Isle of Wight: an overview. Proc. Geol. Assoc. 122, 906–922.
Jongmans, D., Garambois, S., 2007. Geophysical investigation of landslides: a review. Bull. Soc. Geol. Fr. 178 (2), 101–112.
Jongmans, D., Bièvre, G., Renalier, F., Schwartz, S., 2009. Geophysical investigation of a large landslide in glaciolacustrine clays in the Trièves area French Alps. Eng. Geol. 109, 101–112.
Journaux, A., 1971. Formations superficielles et dynamique des versants dans le Pays d'Auge. Colloque International de Géomorphologie, Réunion de la commission d'études des formations superficielles et de la dynamique des versants du Comité National de Géographie, Excursion dans le Pays d'Auge.
Kasser, M., Egels, Y., 2001. Photogrammétrie numérique. Collection ENSG-IGNHermés-Science (379 pp.).
Laudanski, G., Reiffsteck, P., Tacita, J.L., Desanneaux, G., Benoît, J., 2012. Experimental study of drilling parameters using a test embankment. Fourth International Conference on Site Characterization ISC'4, Recife, Bresil, September 2012.
Lissak, C., 2012. Coastal Landslides of the Pays d'Auge (Calvados): Morphology, Functioning and Risk Management. (Ph.D. Thesis) University of Caen, Caen, France.
Lissak, C., Maquaire, O., Malet, J.P., 2010. Multi-technique permanent monitoring of a slow-moving coastal landslide in Normandy. In: Malet, J.P., Remaître, A., Boogard, T. A. (Eds.), Proceedings of the International Conference: 'Mountain Risks: Bringing Science to Society', pp. 267–274.
Lissak, C., Maquaire, O., Puissant, A., Malet, J.P., 2013a. Landslide consequences and post crisis management along the coastal slopes of Normandy, France. In: Margottini, C., Canuti, P., Sassa, K. (Eds.), Landslide Science and Practice. Social and Economic Impact and Policies, vol. 7. Springer, Heidelberg New York Dordrecht London, pp. 23–30.
Lissak, C., Puissant, A., Maquaire, O., Malet, J.P., 2013b. Analyse spatio-temporelle de glissements de terrain littoraux par l'exploitation de données géospatiales multi-sources. Revue Internationale de Géomatique 23, 199–225.
Lissak, C., Maquaire, O., Malet, J.-P., Davidson, R., 2014. Piezometric thresholds for triggering landslides along the Normandy coast, France. Géomorphol. Relief Processus Environ. 2 (in press).
Loke, M.H., 1999. Electrical imaging surveys for environmental and engineering studies. A Practical Guide to 2-D and 3-D Surveys (67 pp.).
Malet, J.P., Maquaire, O., Calais, E., 2002. Le GPS en géomorphologie dynamique. Application à la surveillance de mouvements de terrain Super-Sauze, Alpes du Sud, France. Géomorphol. Relief Processus Environ. 2, 165–180.
Maquaire, O., 1990. Les mouvements de terrain de la côte du Calvados. In: BRGM (Ed.), Recherches et prévention. Documents du BRGM, 197 (430 pp.).
MATE/METL, 1999. Plan de prévention des risques naturels (PPR), Risques de mouvements de terrain. Guide méthodologique, La documentation Française (72 pp.).
Mauritsch, J.H., Seiberl, W., Arndt, R., Römer, A., Schneiderbauer, K., Sendlhofer, G.P., 2000. Geophysical investigations of large landslides in the Carnic Region of southern Austria. Eng. Geol. 56, 373–388.
McInnes, R., 2005. Instability management from policy to practice. In: Glade, T., Anderson, M.G., Crozier, M.J. (Eds.), Landslide Hazard and Risk. John Wiley and Sons, Chichester, pp. 401–428.
McKean, J., Roering, J., 2004. Objective landslide detection and surface morphology mapping using high-resolution airborne laser altimetry. Geomorphology 57, 331–351.
Naudet, V., Lazzari, M., Perrone, A., Loperte, A., Piscitelli, S., Lapenna, V., 2008. Integrated geophysical and geomorphological approach to investigate the snowmelt-triggered landslide of Bosco Piccolo village Basilicata, southern Italy. Eng. Geol. 98, 156–167.
Quantin, C., Allemand, P., Delacourt, C., 2004. Morphology and geometry of Valles Marineris landslides. Planet. Space Sci. 52, 1011–1022.
Razak, K.A., Straatsma, M.W., van Westen, C.J., Malet, J.P., de Jong, S.M., 2011. Airborne laser scanning of forested landslides characterization: terrain model quality and visualization. Geomorphology 126, 186–200.
Schrott, L., Sass, O., 2008. Application of field geophysics in geomorphology: advances and limitations exemplified by case studies. Geomorphology 93, 55–73.
Somerton, W.H., 1959. A laboratory study of rock breakage by rotary drilling. Trans. Am. Inst. Min. Metall. Pet. Eng. 216, 92–97.
Travelletti, J., Malet, J.P., 2012. A methodology for characterizing the 3D geometry of flow-like landslides based on the integration of multi-source data. Eng. Geol. 128, 30–48.
Travelletti, J., Malet, J.P., Hibert, C., Grandjean, G., 2009. Integration of geomorphological, geophysical and geotechnical data to define the 3D morpho-structure of the La Valette mudslide Ubaye Valley, French Alp. In: Malet, J.P., Remaître, A., Boogard, T. (Eds.), Proceedings of the International Conference on Landslide Processes: From Geomorphologic Mapping To Dynamic Modelling. CERG Editions, Strasbourg, pp. 203–208.
Travelletti, J., Demand, J., Jaboyedoff, M., Marillier, F., 2010. Mass movement characterization using a reflexion and refraction seismic survey with the sloping base level concept. Geomorphology 116, 1–10.
Travelletti, J., Malet, J.-P., Samyn, K., Grandjean, G., Jaboyedoff, M., 2013. Control of landslide retrogression by discontinuities: evidences by the integration of airborne- and ground-based geophysical information. Landslides 10, 37–54.
van Den Eeckhaut, M., Verstraeten, G., Poesen, J., 2007. Morphology and internal structure of a dormant landslide in a hilly area: the Collinabos landslide Belgium. Geomorphology 89, 258–273.
van Westen, C.J., 2004. Geo-information tools for landslide risk assessment: an overview of recent developments. Landslide Eval. Stabilization 1, 39–56.